

Simulation Study of Electron and Proton Whistlers in the Ionosphere

Eun-Hwa KIM and Dong-Hun LEE*

Department of Astronomy and Space Science, Kyung Hee University, Yongin 449-701

(Received 23 September 2004)

Electron and proton whistlers are studied in a time-dependent numerical experiment. By adopting the multi-fluid wave model, we investigate the propagation of whistler waves in the mid-latitude ionosphere. Our numerical results show that proton whistlers appear on the dynamic spectrum as rising tones, which start after the reception of a short electron whistler, asymptotically approaching the proton gyro-frequency. The time histories and the dynamic spectra of the electric fields at different altitudes are presented. A polarization reversal is found to continuously occur at the crossover frequencies as the altitude increases. Our simulation confirms that the proton whistler and the electron whistler are left- and right-handed circularly-polarized waves, respectively.

PACS numbers: 84.40.Ik, 84.40.Fe

Keywords: Polarization reversal, Whistler

I. INTRODUCTION

The inclusion of multi-ions in the plasma facilitates the propagation of left-handed circularly-polarized (LHP) waves for the band of frequencies below each ion gyro-frequency. Smith and Brice [1] found that between two adjacent ion gyro-frequencies there is a frequency, called the crossover frequency (ω_{cr}), where the mode becomes linearly polarized, and both the LHP and right-handed circularly-polarized (RHP) modes are exchanged beyond the cross-over location. Thus, when the frequency approaches ω_{cr} , polarization reversal occurs.

In the ionosphere, polarization reversal provides a mechanism by which upgoing electron whistlers can become proton whistlers. Proton whistlers are dispersed forms of lightning impulses observed in the ionosphere, and appear on the dynamic spectrum as rising tones asymptotically approaching the local proton gyro-frequency (see, *e.g.*, [1] and [2]). Barrington *et al.* [3] and Gurnett and Rodriguez [4] observed similar phenomena near the helium gyro-frequency, which they called a helium whistler.

The polarization reversal and the mode coupling of electron and proton whistlers have been discussed by several workers [5–7]. According to Gurnett *et al.* [2], strong mode coupling exists when the RHP electron whistlers are split into both RHP and LHP waves, both of which appear simultaneously in observations (we use their definition of *mode coupling* hereafter). Gurnett *et al.* [2] were able to explain the polarization reversal of proton whistlers at ω_{cr} in a collisionless model. They also suggested that collisions should be important in mode cou-

pling to explain the occurrence of both electron and proton whistlers. Recently, Ferencz [8] suggested that ion cyclotron whistlers may occur in the case of longitudinal propagation, as well as oblique propagation, without assuming any kind of polarization reversal or mode coupling when waves start at the mid-altitude ionosphere. An experimental study of polarization reversal and mode coupling of electron and proton whistlers was performed by Rodriguez and Gurnett [9]. They considered five types of whistlers: polarization reversal and no coupling (type C₁), polarization reversal and weak coupling (type C₂), strong coupling (type C₃), no polarization reversal and weak coupling (type C₄), and no polarization reversal and no coupling (type C₅).

It is purpose of this letter to report on the first numerical simulation of electron and proton whistlers in a time-dependent manner. By adopting a multi-fluid numerical model, we reproduce whistler waves. With the group travel time calculated analytically, our simulation results show how electron and proton whistlers propagate in the mid-latitude ionosphere. We also compare our results with those of previous observational and theoretical studies.

II. DISPERSION RELATION

Figure 1 shows the dispersion relation in the presence of helium ions when k_{\perp} is constant, where k_{\perp} is the wavevector perpendicular to the background magnetic field (\vec{B}_0). In this figure, the three branches of the dispersion relation are referred to as class I, II, and III. Class I waves have frequencies below the helium gyro-frequency (ω_{cHe}), and they are LHP waves. Class II and III waves

*E-mail: dhlee@khu.ac.kr

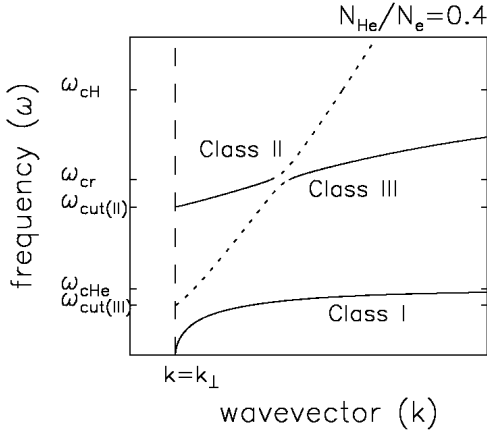


Fig. 1. Dispersion relation of plasma waves in the presence of He ions (here $N_{\text{He}}/N_e = 0.4$). The solid curves and the dotted curves denote LHP and RHP waves, respectively. Note the polarization reversal at $\omega = \omega_{cr}$.

have frequencies $\omega_{\text{cut(II)}} < \omega$ and $\omega_{\text{cut(III)}} < \omega < \omega_{\text{cH}}$, respectively, where $\omega_{\text{cut(II)}}$ and $\omega_{\text{cut(III)}}$ are the cut-off frequency of LHP Class II and RHP Class III, respectively, and ω_{cH} is the hydrogen gyro-frequency. Since we assume a finite wavevector (k) in our simulation, the cut-off condition is reduced to $n_{\parallel}^2 = 0$. The crossover frequencies are the frequencies at which the refractive indices of two characteristic modes become equivalent.

The polarization reversal at ω_{cr} is visualized in Fig. 1. The solid and the dotted curves denote LHP and RHP waves, respectively. For Class II, the LHP mode branch beginning at $\omega_{\text{cut(II)}}$ becomes a RHP mode at ω_{cr} . Class III waves consist of the LHP mode for $\omega_{cr} < \omega < \omega_{\text{cH}}$ and the RHP mode for $\omega < \omega_{cr}$. In the ionosphere, the polarization reversal of Class III waves becomes important in the generation of proton whistlers.

III. MODEL

In a cold plasma, linearized plasma waves can be described by Maxwell Equations and the Equation of motion for a single particle of species j :

$$\vec{\nabla} \times \vec{E} = -\frac{\partial \vec{b}}{\partial t}, \quad (1)$$

$$\vec{\nabla} \times \vec{b} = \mu_o \vec{J} + \frac{1}{c^2} \frac{\partial \vec{E}}{\partial t}, \quad (2)$$

$$N_j m_j \frac{\partial \vec{V}_j}{\partial t} = N_j q_j (\vec{E} + \vec{V}_j \times \vec{B}_0), \quad (3)$$

$$\vec{J} = \sum_j N_j q_j \vec{V}_j, \quad (4)$$

where \vec{E} , \vec{b} , \vec{V} , and \vec{J} represent the perturbed electric and magnetic fields, the velocity, and the current density, respectively. We adopt a box model which is based

on that of Kim and Lee [10]. The ambient magnetic field and the inhomogeneity are assumed to lie in the z direction. We limit ourselves to harmonic variations in the x direction (perpendicular to the magnetic field), and all waves are proportional to $\exp(ik_x x)$, where k_x is the given x direction wavenumber. Since hydrogen and helium ions have predominant concentrations in the topside ionosphere, we assume an electron-hydrogen-helium plasma. To save computing time, the proton-to-electron mass ratio is assumed to be 100. In this model, frequencies are normalized to ω_{cH} ($\Omega = \omega/\omega_{\text{cH}}$), time is normalized to $t_{\text{cH}} = 1/\omega_{\text{cH}}$, and length is normalized to $\lambda_{\text{cH}} = c/\omega_{\text{cH}}$. We assume the maximum altitude to be $L_z = 70\lambda_{\text{cH}}$ in this model. The simulation is run from $t = 0$ to $t = 2638t_{\text{cH}}$. An impulsive input is assumed for E_y at $z = 0$ during $0 < t < 1.76t_{\text{cH}}$, which is similar to a lightning impulse at the ground. For convenience, we assume a single wave vector $k_x = 1.07/\lambda_{\text{cH}}$, which can include the effect of slanting propagation with respect to the magnetic field such as in the mid-latitude ionosphere. The boundaries are assumed to become perfect reflectors after the impulsive stimulus ends.

We focus on the effect of crossover. The crossover frequency between hydrogen and helium gyro-frequencies is given by

$$\omega_{cr} = \alpha \omega_{\text{cHe}}^2 + \beta \omega_{\text{cH}}^2, \quad (5)$$

where $\alpha = N_{\text{H}}/N_e$ and $\beta = N_{\text{He}}/N_e$. Since ω_{cr} is affected by the ion concentration ratio shown in Eq. (5), to investigate wave properties between two ion gyro-frequencies easily, we assume that B_0 and N_e are constant and that the ion concentration parameters α and β vary along the z direction. Figure 2(a) shows the ion concentration parameter profiles assumed in this study. The relative concentration of hydrogen increases as the altitude increases in the z direction. Using the ion density profiles in Fig. 2(a), the normalized crossover (Ω_{cr}) and cut-off frequencies (Ω_{cut}) have been plotted as functions of the altitude in Fig. 2(b). Ω_{M} denotes the maximum of the crossover frequency. In this figure, the shaded region represents the cut-off for LHP waves. Thus, near $\xi=0$, Class II LHP waves with Ω in the range $\Omega_{\text{cHe}} < \Omega < \Omega_{\text{cut(II)}}$ cannot propagate while LHP Class II waves with Ω in the range $\Omega_{\text{cut(II)}} < \Omega < \Omega_{cr}$ and LHP Class III waves with Ω in the range $\Omega_{cr} < \Omega < \Omega_{\text{cH}}$ can propagate to higher altitude.

IV. GROUP TRAVEL TIME

The group travel time (τ) of a proton whistler from the source of the lightning impulse to a satellite is given by the line integral

$$\tau(\omega) = \int_s \frac{1}{v_g} ds', \quad (6)$$

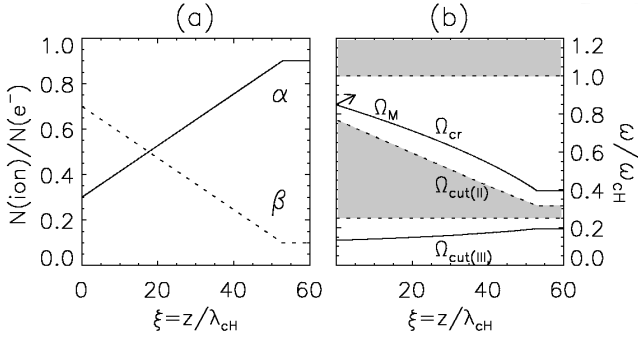


Fig. 2. (a) Ion concentration parameter profile, $\alpha = N_{\text{H}}/N_e$ and $\beta = N_{\text{He}}/N_e$. (b) The normalized crossover (Ω_{cr}) and Ω_{cut} frequencies. Ω_M denotes the maximum of Ω_{cr}

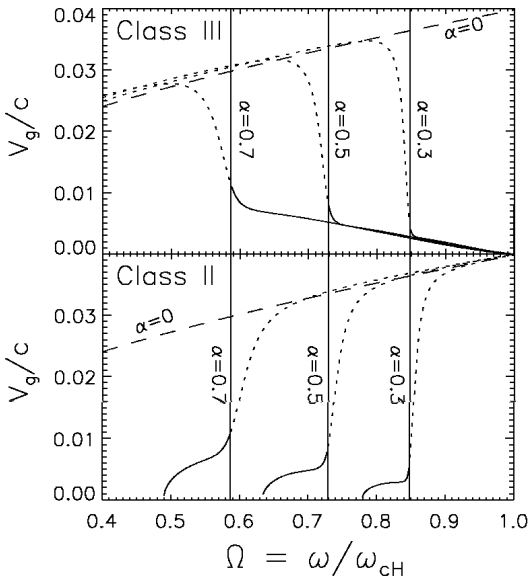


Fig. 3. Group velocities of Class II and III waves as functions of frequency. The solid and the dotted curves denote LHP and RHP waves, respectively.

where v_g is the group velocity along the ray path s . The group velocities and the integral in Eq. (6) are based on the ion concentration profile in Fig. 2. Figure 3 shows the group velocities of Class II and III waves for various α . In that figure, the dotted and the solid lines represent RHP and LHP waves, respectively. The vertical lines denote the crossover frequencies for each α . The group velocities become zero near the cut-off frequencies for Class II and near ω_{CH} for Class III. The group velocities of LHP waves are much smaller than those of RHP waves in Fig. 3. The RHP waves have minimum group velocities around ω_{cr} , which correspond to the maximum group velocities of the LHP waves.

Figure 4 shows the computed group travel time (τ) as a function of frequency at $\xi = 17.59$ and 35.17 . We assume that the source is given at $\xi = 0$ around $\tau = 0$. The helium cyclotron wave and the electron and the proton whistlers appear in Fig. 4, and they correspond to Class

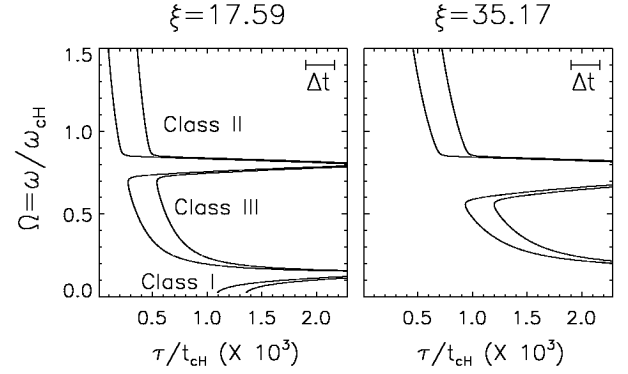


Fig. 4. Computed group travel time (τ) at $\xi = 17.59$ and 35.17 .

I, II, and III in Fig. 1, respectively.

Class I waves represent the helium cyclotron waves at $\xi = 17.59$. This mode starts near the end of the electron whistler and shows a rise in frequency. Since the group velocity of Class I is much smaller than the group velocities of Class II and III, helium cyclotron waves do not appear at $\xi = 35.17$. Class II shows the fractional-hop electron whistler for $\Omega > \Omega_M$. Class III shows the electron and the proton whistlers. The proton whistler appears simultaneously with the electron whistler. The band gap between the two electron whistlers of Class II and Class III is caused by the crossover frequency range, which is given by $\Omega_{\text{cr}} = 0.73$ and 0.59 at $\xi = 17.59$ and 35.17 , respectively. Where the crossover condition is satisfied, the wave polarization changes from an electron RHP whistler to a proton LHP whistler. Since LHP waves have a group velocity with a maximum at Ω_{cr} , they start immediately at the local Ω_{cr} and show a rise in frequency. Since the RHP Class III waves are converted into LHP Class III and since RHP Class II waves having $\Omega < 1$ cannot propagate to higher altitude, a frequency gap of electron whistlers occurs. These computed group-travel-time curves for the electron and the proton whistlers are in good quantitative agreement with the previous analytical results [2].

V. NUMERICAL RESULTS

Time histories of the electric field at a line of grid points along ξ were recorded. Figure 5 presents the time histories of E_x at $\xi = 5.86, 11.72, 17.59, 23.45, 29.31,$ and 35.17 . In Fig. 5, it is evident that the dispersion period (length of the wave train) grows significantly with ξ and that the delay time interval increases monotonically with ξ . Figure 6 shows the dynamic spectra of $E_x, E_R,$ and E_L at $\xi = 17.59,$ and 35.17 , where E_R and E_L are the RHP and the LHP electric field components [11] defined as

$$E_R = (E_x^a + jE_y^a)/2, \quad (7)$$

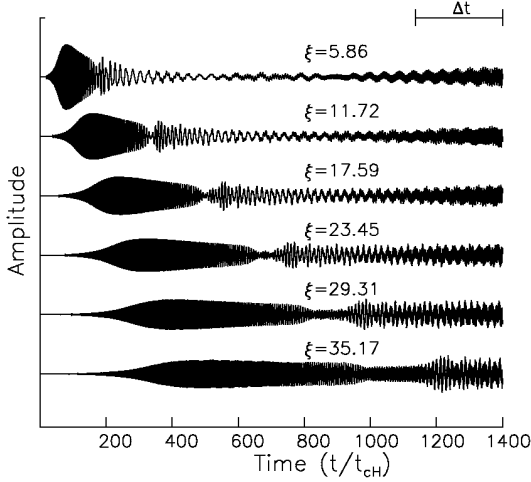


Fig. 5. Time histories of E_x at $\xi = 5.86, 11.72, 17.59, 23.45, 29.31,$ and 35.17 .

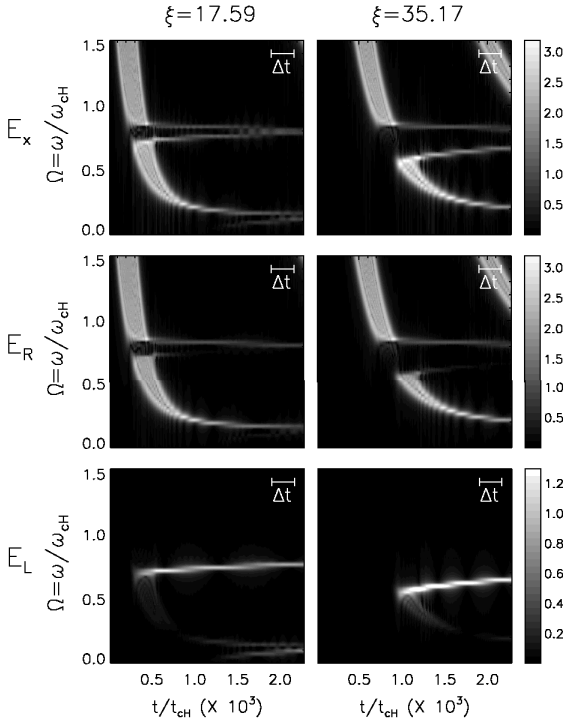


Fig. 6. Dynamic spectra of E_x , E_R , and E_L at $\xi = 17.59$ and 35.17 .

$$E_L = (E_x^{a*} + jE_y^{a*})/2, \quad (8)$$

where the asterisk denotes the complex conjugate. E^a is an analytic signal defined as $E^a = E_{x(y)} + j\tilde{E}$, where \tilde{E} is the Hilbert transform of E . The Hilbert transform is equivalent to a kind of filter, which gives differential phase shifts ($\pm \pi/2$) according to the positive and negative sense of rotation. To obtain the dynamic spectrum, we Fourier transformed the time series at each location (Fig. 5) with a period of Δt .

The dynamic spectra of E_x in Fig. 6(a) are found

to correspond to the computed travel time of Fig. 4 in timing and frequency. E_x shows a fractional-hop electron whistler and a proton whistler. Figure 6 suggests that polarization reversal occurs at the local Ω_{cr} ; thus, the frequency gap of electron whistlers appears in the range $\Omega_{cr} < \Omega \leq \Omega_M$. Our results are found to be consistent with type C_1 of Rodriguez and Gurnett's classification [9].

The helium cyclotron waves are shown at $\xi = 17.59$ in Fig. 6. Since we assumed the boundary to be a perfect reflector, the reflected electron whistlers appear only in the dynamic spectrum at $\xi = 0$. In Fig. 6, E_R shows the electron whistler while E_L shows the proton whistlers and the helium cyclotron wave. It is evident that the electron whistlers are RHP waves and the proton whistlers are LHP waves. Smith [12] separated whistler mode waves into RHP and LHP components by using the Ogo 6 satellite. Those experimental polarization measurements are consistent with our results.

In both Figs. 4 and 6, the unique RHP mode is found near Ω_M and comes from the polarization reversal of Class II LHP modes between $\Omega_{cut(II)} < \Omega < \Omega_M$ in the beginning. In the lower ionosphere is the LHP wave cut-off region between the helium and the hydrogen gyro-frequencies; thus, unlike other LHP and RHP modes above, this branch is not found in observations.

VI. SUMMARY AND DISCUSSION

The frequency spectrum of a proton whistler is explained by considering electromagnetic waves in the ionosphere of multi-ions. By adopting the multi-fluid numerical wave model, we reproduced electron and proton whistler waves in the mid-latitude ionosphere. Even if we adopt a simple ion concentration profile, our numerical results are strongly consistent with those of previous observational and theoretical studies. Our results also confirm that proton and electron whistlers are LHP and RHP modes, respectively.

There are several limitations in our study presented here. We assumed that the electron density was constant in altitude. Inhomogeneities in the total electron density should be important in coupling and mode conversion among the different wave modes. However, we focused on the effect of crossover in this paper. We showed how polarization reversal occurs with a crossover condition between electron and proton whistlers. Our results should help us understand and differentiate the polarization reversal in observations from mode coupling which can be caused by several factors such as nonconformity, finite temperature, and collisions.

In Gurnett *et al.*'s definition of mode coupling [2], strong mode coupling may split the RHP waves into two circularly polarized waves at the local crossover frequency. According to their definition, there is no mode coupling in our results owing to the fact that we as-

sume no collisions among multi-ions and electrons in our model. Since our model is based on the collisionless fluid model, our results should be supplemented by the effects of collisions [2], cyclotron damping [13], and warm plasmas [14]. These subjects will be left as our future work.

ACKNOWLEDGMENTS

This work was supported by the Korea Science & Engineering Foundation grant R14-2002-043-01000-0.

REFERENCES

- [1] R. L. Smith and N. Brice, *J. Geophys. Res.* **69**, 5029 (1964).
- [2] D. A. Gurnett, S. D. Shawhan, N. M. Brice and R. L. Smith, *J. Geophys. Res.* **70**, 1665 (1965).
- [3] R. E. Barrington, J. S. Belrose and W. E. Mather, *Nature* **210**, 80 (1966).
- [4] D. A. Gurnett, and P. Rodriguez, *J. Geophys. Res.* **75**, 1342 (1970).
- [5] D. Jones, *J. Atmos. Terr. Phys.* **31**, 971 (1969).
- [6] D. Jones, *Ann. Geophys.* **28**, 527 (1972).
- [7] T. I. Wang, *J. Geophys. Res.* **76**, 947 (1971).
- [8] O. E. Ferencz, in *Whistler Phenomena*, edited by C. Ferencz, O. E. Ferencz, D. Hamar and J. Lichtenberger, (Kluwer Academic Publishers, Dordrecht, 2001), p. 96.
- [9] P. Rodriguez and D. A. Gurnett, *J. Geophys. Res.* **76**, 960 (1971).
- [10] E.-H. Kim and D.-H. Lee, *Geophys. Res. Lett.* **30**, 2440, doi:10.1029/2003GL017918 (2003).
- [11] K. Kodaera, R. Gendrin and C. De Villedary, *J. Geophys. Res.* **82**, 1245 (1977).
- [12] R. L. Smith, *J. Geophys. Res.* **75**, 7261 (1970).
- [13] D. A. Gurnett and N. M. Brice, *J. Geophys. Res.* **71**, 3639 (1966).
- [14] A. K. Singh, A. K. Singh, D. K. Singh and R. P. Singh, *J. Atmos. Solar-Terr. Phys.* **60**, 551 (1998).